

Vibrational modes and diffusion of self-interstitial atoms in body-centered-cubic transition metals: A tight-binding molecular-dynamics study

Daniel Finkenstadt,^{1,2,*} N. Bernstein,¹ J. L. Feldman,^{2,1} M. J. Mehl,¹ and D. A. Papaconstantopoulos^{2,1}

¹*U.S. Naval Research Laboratory, 4555 Overlook Avenue, SW, Washington, DC 20375, USA*

²*George Mason University, School of Computational Sciences, 4400 University Drive, Fairfax, Virginia 22030, USA*

(Received 10 May 2006; revised manuscript received 18 September 2006; published 28 November 2006)

Using a tight-binding molecular-dynamics method, we have calculated the formation energies, diffusivity, and localized vibrational frequencies of self-interstitial atoms (SIA's) in body-centered-cubic (bcc) transition metals: vanadium, niobium, molybdenum, and tantalum. As a test of our methods, we compare to experiment for the perfect bcc phonon spectra and we compare to previous *ab initio* SIA formation energies. In addition, we present vibrational spectra calculated from molecular dynamics via the velocity autocorrelation method. For all of the systems studied, we find that the localized vibration frequency of a SIA dumbbell pair is roughly twice the frequency of the bcc phonon-density-of-states peak. We also find an Arrhenius temperature dependence for SIA hopping, with frequency prefactors ranging between the cutoff of the ideal bcc lattice and the highest frequencies of the SIA dumbbell. In all cases, we find that the energy barrier to SIA diffusion is approximately 0.1 eV.

DOI: [10.1103/PhysRevB.74.184118](https://doi.org/10.1103/PhysRevB.74.184118)

PACS number(s): 61.72.Ji, 63.20.Pw, 66.30.Fq, 71.20.Be

I. INTRODUCTION

Traditionally, the self-interstitial atom (SIA) has been difficult to study experimentally, due to the high mobility¹ and low concentration of SIA's, except in irradiated materials.² This difficulty has propelled study by *ab initio* and semi-empirical computational methods³ to explore the formation energetics and diffusion modes of SIA's and clusters of SIA's in many bcc transition metals: V,^{4–8} Fe,^{9–14} Nb,⁸ Mo,^{4,8,15–17} Ta,^{8,18} and W.^{8,19,20} These findings mostly confirm the stability of SIA dumbbell configurations and predict SIA motion along high-symmetry directions. In the present work, we will expand on the most recent of these findings and reexamine an earlier work,^{15,16} which suggested the possibility of localized SIA vibrational modes, mostly decoupled from the eigenmodes of the host lattice. We will show that such high-frequency modes do, in fact, occur in many bcc systems and that these modes likely explain previous calculations for enhanced high-frequency tails in phonon spectra due to SIA's.^{12,21} We find a high mobility of SIA's in V and Mo, which agrees with previous work,^{4,6} as well as in Nb and Ta, suggesting that this is a generic feature of bcc transition metals. To do this we use the NRL tight-binding method,^{22–27} an efficient electronic-structure method utilizing parameters fit to first-principles data,²⁸ in combination with molecular dynamics.^{29,30}

The calculations presented here compute, within a tight-binding framework, the diffusivity of single SIA's and their quantitative effect on the vibrational density of states (VDOS) in metals. While previous works have established accurate methods for calculating static properties and some migration energy pathways, as in Ref. 8, these same methods are not practical for calculating hopping and molecular dynamics of SIA's that are often addressed by less accurate interatomic potential methods, as in Refs. 6 and 7. Here we show that a tight-binding framework can address both the static properties, by reproducing the stable SIA energies, and also efficiently treat the hopping of SIA's within molecular

dynamics. We also expand on previous works that mention high-frequency tails in phonon spectra with clusters of SIA's.¹² We calculate spectra for bcc transition metals with and without SIA's, and we identify the specific SIA modes contributing to the identified peaks. We report a uniform trend that SIA's vibrate at roughly twice the frequency of their perfect bcc VDOS peaks, and we also show that the frequency prefactor for hopping lies above the frequency cutoff of the ideal bcc lattice. For comparison with previous expectations that low-frequency modes are mostly responsible for the glide motion of SIA's,¹² we illustrate how the fast dumbbell-axial vibrations, compared to the slow center-of-mass motions, contribute to SIA hopping.

The paper is organized as follows. In Sec. II, we describe the methods for tight-binding parametrization and for molecular-dynamics (MD) simulation. We also present the velocity autocorrelation method for calculating dynamical properties. In Sec. III, we present results for both static properties (SIA formation energy and structure) and dynamical properties (SIA diffusion rates and localized vibrational modes). We also discuss how SIA's might affect vibrational spectra in experimental systems under pressure—namely, hexagonal iron.³¹ In Sec. IV we summarize these results, followed by an Appendix on the phonon dispersion relations obtained from our tight-binding parametrization, compared to experiment, as a test of our methods.

II. METHODS

The SIA is one of two basic kinds of structural point defects, the other being the atomic vacancy. When two atoms try to share a single-crystal lattice site (see Fig. 1), then various types of split “dumbbell” configurations can occur.³² In bcc crystals, the metastable SIA configurations are distinguished by the high-symmetry directions of the vector \mathbf{s} in Fig. 1—namely, $\langle 100 \rangle$, $\langle 110 \rangle$ and $\langle 111 \rangle$. Of course, after relaxation of the structure, many of these configurations may equally well be described by a so-called “crowdion”

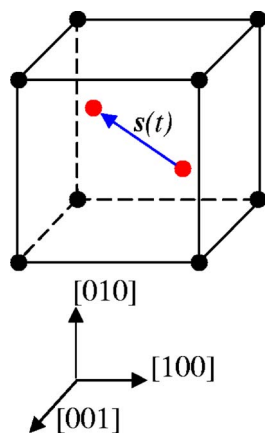


FIG. 1. (Color online) Self-interstitial atom (SIA) configurations in a bcc traditional cell. Two atoms share the body center. The vector $s(t)$ describes the SIA bond, as a function of time t . The dumbbell center of mass also varies with time.

configuration,³³ where three atoms try to share two lattice sites or five share four, etc. In all cases, however, the ideal (undefected) crystal can be partitioned into Wigner-Seitz cells so that the location of a SIA is uniquely determined as the Wigner-Seitz cell that contains an excess atom. Based on this, an initial SIA structure can be generated, and as the MD progresses, the SIA is continually tracked by counting the number of atoms in each Wigner-Seitz cell. Thus, at every time step, the vector $s(t)$ is updated along with the SIA dumbbell center of mass. In the following, we will outline the computational procedures for performing this type of SIA simulation and the methods for analyzing dynamical properties.

A. Tight binding for self-interstitial atoms

Several empirical potential methods have been applied to the SIA, notably the embedded-atom method^{34,35} (EAM, applied, e.g., in Ref. 36) and the Finnis-Sinclair potentials³⁷ (FS potentials, applied, e.g., in Ref. 7). While generally less accurate than explicit electronic-structure methods, empirical potential models do not break down at close atomic separations, which occur normally in the vicinity of a SIA. However, empirical potentials may be even less accurate at these close separations. Similarly, at the high end of first-principles accuracy density-functional theory³⁸ (DFT) methods, such as the linearized augmented plane-wave^{39,40} (LAPW) or pseudopotential⁴¹ methods, come at a high computational cost and are not suitable for long MD runs with a large number of atoms. For a robust approach that is much faster than DFT, combined with the accuracy of calculating electronic structure from first principles, we choose the NRL tight-binding method^{22–27} (TB) in combination with molecular dynamics (TBMD).^{29,30}

The TB method gives accurate electronic structure for a broad range of materials,^{24,25,42} including transition metals,²³ and for dynamical properties at finite temperature.²⁹ In this work, we find that the TB method gives stable bcc structures for all of the transition metals examined. Our TB parameters are fit to high-accuracy LAPW results for both equilibrium

and reduced-lattice constant structures, so that we accurately describe SIA formation energies. For all SIA static calculations, we use a $[128(+1)]$ -atom cell, with a $4 \times 4 \times 4$ Monkhorst-Pack⁴³ k -point sampling of the Brillouin zone, and we relax ionic coordinates and volume to reduce Hellman-Feynman forces to <20 meV/Å. The equilibrium lattice constant was calculated here to be 2.93(3.27, 3.12, 3.30) Å, compared to the experimental value⁴⁴ of 3.02(3.30, 3.15, 3.31) Å for V (Nb, Mo, Ta). These comparisons reflect the well-known tendency of local-density approximation³⁸ (LDA) to underestimate lattice spacings in many systems—e.g., as shown in Al and Ag using two different electronic-structure methods.⁴⁵

In cases where the TB parameters are poorly fit, the SIA often becomes unstable to close separation. As a function of decreasing separation, these unphysical results can occur just before nonpositive-definite overlap integrals are returned. This feedback from the simulation indicates which of the parameters might produce unphysical interactions, unlike the EAM or FS potentials that are *a priori* tolerant to any separation. Details of our TB parametrization, convergence, and tests versus experiment of the bcc VDOS are given in the Appendix.

B. Molecular dynamics and velocity autocorrelation

For our MD simulation of the SIA, a large cell was required to relax the large lattice strain in the vicinity of the defect. In previous studies,⁴ as few as 54(+1) atoms were sufficient to converge SIA formation energies to ± 0.1 eV. For our MD simulation, we chose a repeated traditional bcc unit cell (two-atom basis, repeated 4 times per direction) containing 128 atoms, plus one SIA.

Since the tight-binding-calculated linear thermal expansion coefficients are small,⁴⁶ about $5 \times 10^{-6}/\text{K}$, we neglect the contributions of thermal expansion and use the equilibrium lattice constants for all of our finite-temperature MD simulations. This is justified for the bcc transition metals that we study, because the lattice constants are not altered appreciably except near the melting point in each system. As an example, we expect a maximum of 1% linear expansion for $T < 2000$ K. For comparison, the experimental coefficients⁴⁷ are $8(7, 5, 6) \times 10^{-6}/\text{K}$ for V (Nb, Mo, Ta), giving 1% expansion for temperatures between 1250 K and 2000 K.

To minimize the computational cost of long MD runs, the Γ point *only* was used for Brillouin zone k -point sampling during the MD simulations. Random velocities were chosen to achieve the desired equilibrium temperature. In all systems, the MD were run for 16 384 time steps of $\Delta t = 2.0$ fs, giving a total simulation time of 33 ps. The first 2000 time steps were discarded for thermal equilibration, and the remaining steps were kept and used for analysis of dynamical properties.

To analyze phonon and other dynamical properties, we used the velocity-autocorrelation (VAC) method, as derived in Ref. 48 and applied more recently to MD computed vibrational spectra.⁴⁹ The VAC method is essentially a time-domain Fourier transform of velocity-related quantities—namely, $\sum_i \langle \mathbf{v}_i(t) \cdot \mathbf{v}_i(0) \rangle$ for obtaining the VDOS, using the

TABLE I. Self-interstitial formation energies ΔE_f (in eV, ± 0.1 eV). We compare our current tight-binding (TB) results to *ab initio* pseudopotential calculations (previous) for nonmagnetic cases (Ref. 8) and for ferromagnetic Fe (Ref. 13). The axial vector \hat{s} , in Fig. 1, is reported in units of the host lattice interatomic spacing.

	s	TB \hat{s}	ΔE_f	Previous ΔE_f
V	0.83	$\langle 100 \rangle$	4.25	3.92
	0.83	$\langle 110 \rangle$	4.35	3.65
	0.84	$\langle 111 \rangle$	4.25	3.37
Nb	0.84	$\langle 100 \rangle$	4.80	5.95
	0.84	$\langle 110 \rangle$	4.85	5.60
	0.86	$\langle 111 \rangle$	4.60	5.25
Mo	0.85	$\langle 100 \rangle$	8.95	9.00
	0.85	$\langle 110 \rangle$	7.85	7.58
	0.86	$\langle 111 \rangle$	7.70	7.42
Ta	0.85	$\langle 100 \rangle$	4.85	7.00
	0.84	$\langle 110 \rangle$	4.80	6.38
	0.86	$\langle 111 \rangle$	4.25	5.83
Fe	0.67	$\langle 100 \rangle$	2.30	4.64
	0.67	$\langle 110 \rangle$	1.60	3.64
	0.70	$\langle 111 \rangle$	1.80	4.34

site velocities $\mathbf{v}_i(t)$, or $\langle v_{\mathbf{k}}^\alpha(t)v_{\mathbf{k}}^\alpha(0) \rangle$ for obtaining the dispersion relations, using the spatially Fourier transformed velocities $v_{\mathbf{k}}^\alpha(t)$ with wave vector \mathbf{k} and polarization α . For comparison of the VAC method to frozen phonon results and experiment; see the Appendix.

For the special aspects of the vibration of the SIA, we can take the bond-length and center-of-mass (COM) degrees-of-freedom of a dumbbell, using the $\mathbf{v}_i(t)$ for both atoms. Because the pair can point in all directions, we must carefully consider which modes we are projecting out in our analysis. In the case of a dumbbell pointing in an arbitrary direction, but centered on a lattice site, the only guaranteed symmetry will be the identity and an inversion point, giving A_g and A_u modes. With a harmonic approximation, the localized bond-stretching modes will vibrate with A_g frequencies. Therefore we will refer to the bond-stretching mode, as in a dimer molecule, by the A_g designation. For higher-symmetry dumbbell orientations, the A_g designation remains valid but the eigenmodes may be different—e.g., as for the D_{4h} , D_{2h} , and D_{3d} symmetries of the $\langle 100 \rangle$ -, $\langle 110 \rangle$ -, and $\langle 111 \rangle$ -oriented dumbbells, respectively.^{15,16} To avoid restricting ourselves to any one symmetry, we will analyze the degrees of freedom common to all dumbbell orientations, and we will Fourier analyze the correlations $\langle \dot{s}(t)\dot{s}(0) \rangle$ and $\langle \mathbf{v}_{c.m.}(t) \cdot \mathbf{v}_{c.m.}(0) \rangle$, where $\dot{s}(t)$ is the time derivative of the dumbbell bond length, in Fig. 1, and $\mathbf{v}_{c.m.}$ is the COM velocity of a split-interstitial pair.

III. SELF-INTERSTITIAL STATIC AND DYNAMIC PROPERTIES

As a preliminary check on our methods, we first calculated the SIA formation energies ΔE_f , with ionic and volume

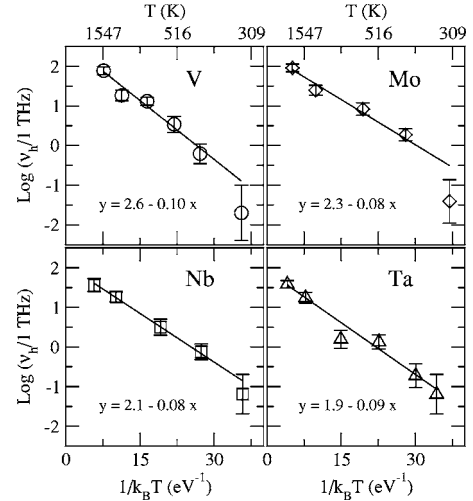


FIG. 2. Arrhenius plot for self-interstitial hopping in bcc transition metals. The slope of each linear fit is ΔE_m from Eq. (2), in eV. The intercept is a function of the Arrhenius prefactor—namely, $\log(\nu_a/1 \text{ THz})$.

relaxations. The quantities ΔE_f were calculated for an N -atom cell, plus one interstitial, as

$$\Delta E_f = E_{SIA}(N+1) - \frac{N+1}{N} E_{bcc}(N), \quad (1)$$

where E_{SIA} and E_{bcc} are the defected and bulk formation energies, respectively. The results for ΔE_f are listed in Table I. Our ΔE_f are within 1 eV of the previous results for most cases, except for Ta, for which we find the ΔE_f are 1.5–2 eV below the previous calculations,⁸ and Fe, which we will discuss below. Also for V, the $\langle 100 \rangle$ energy is clearly low, compared to the $\langle 111 \rangle$ energy. However, even for pseudopotentials,⁴ the $\langle 100 \rangle$ – $\langle 111 \rangle$ energy difference for V is only one-third as large as that for Mo or Ta. A similarly small $\langle 100 \rangle$ – $\langle 111 \rangle$ energy is found for Nb.⁸ The existence of a nearly stable $\langle 100 \rangle$ configuration favors “traditional interstitials” that we will discuss in the following section. Despite the discrepancies in $\langle 100 \rangle$ energies, our $\langle 110 \rangle$ – $\langle 111 \rangle$ energy differences are virtually identical to the previous calculations for Nb, Mo, and Ta,^{4,8} and the relative orderings for all of our nonmagnetic systems are consistent with the previous find-

TABLE II. Self-interstitial hopping data at $T > 300$ K, fit to Arrhenius form [Eq. (2)]. The prefactors ν_a are from Fig. 2, and the dumbbell bond-frequencies ν_{A_g} are from Fig. 4 (in THz). The energy barriers for migration, ΔE_m (in eV), are compared to previous pseudopotential calculated energy barriers for V (Ref. 4) and for (54+1)-atom Ta (Ref. 18) and from experiment for Mo (Ref. 2).

	ν_a	TB ν_{A_g}	ΔE_m	Previous ΔE_m
V	14.0 ± 2.5	18.3	0.10 ± 0.10	0.01
Nb	8.1 ± 1.0	11.8	0.08 ± 0.01	
Mo	10.1 ± 1.5	14.7	0.08 ± 0.01	0.05
Ta	6.9 ± 1.0	8.2	0.09 ± 0.01	0.60

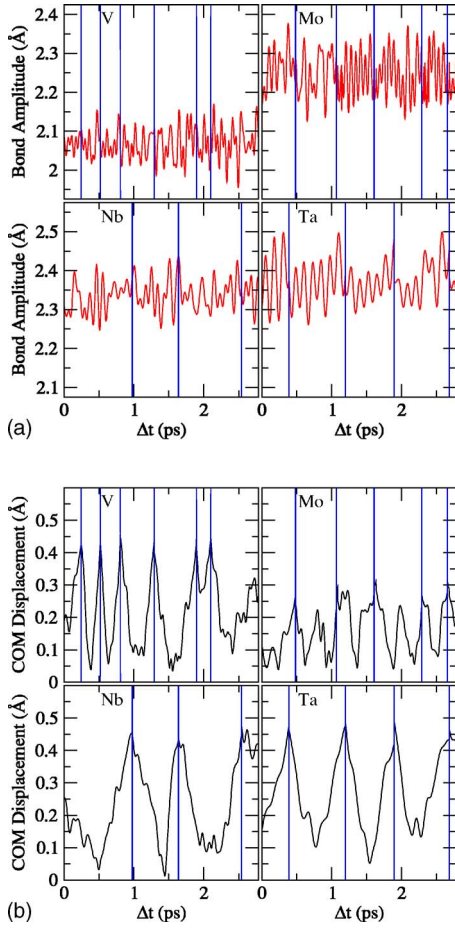


FIG. 3. (Color online) Trajectories of self-interstitial dumbbell bond A_g modes (a) and center of mass (b) at 400 K. Vertical lines indicate hopping events.

ings that $\langle 111 \rangle$ is the lowest-energy orientation.

As an additional comparison for a magnetic case, we briefly mention here our preliminary results for ferromagnetic Fe, also listed in Table I. Currently, our results for ΔE_f in Fe, lie more than 2 eV below the most recent *ab initio* results,¹³ but we confirm that the $\langle 110 \rangle$ -oriented dumbbell has the lowest energy, 0.2 eV below the $\langle 111 \rangle$ case, compared to 0.7 eV from previous studies.^{11,13} Similarly, the $\langle 100 \rangle$ dumbbell lies 0.5 eV above the $\langle 111 \rangle$ energy, compared to 0.3 eV from the previous work. The reversed ordering of the $\langle 111 \rangle$ and $\langle 110 \rangle$ cases, compared to the nonmagnetic cases, is in agreement with previous *ab initio* predictions.^{11,13}

A. Self-interstitial diffusion

Having checked the static values for ΔE_f , we now turn to MD simulation to obtain the hopping rates for SIA migration. Following the procedure described in Ref. 6, we count the rate ν_h of hopping events into neighboring Wigner-Seitz cells, as a function of temperature. This procedure gives a reasonable temperature dependence of the hopping frequency for Mo and Ta. However, for V and Nb, we recognize anomalously high count rates, for $T < 600$ K, caused by SIA's occurring not as dumbbells, but rather in traditional

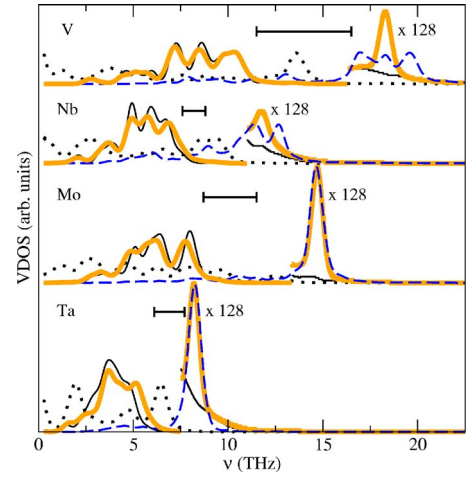


FIG. 4. (Color online) Vibrational density of states (VDOS) for bcc transition metals and self-interstitial atoms (SIA) at 400 K. The orange (gray) solid line is the VDOS with SIA, while the thin black line is the VDOS without SIA, and the tails are enhanced $\times 128$. The dashed (dotted) lines are the localized A_g (resonant COM vibration) modes of the split-dumbbell interstitial. The prefactors from Table II are shown as cross bars.

hole sites. As mentioned above, V and Nb have small energy differences between the $\langle 100 \rangle$ and $\langle 111 \rangle$ dumbbells. This low energy allows dumbbells to rotate easily into a $\langle 100 \rangle$ direction, sometimes with one atom centered on the octahedral hole site. Since these hole sites lie between two cells, they can register a number of false SIA hops and we subtract out those counts. The resulting, corrected data are shown in Fig. 2 and exhibit a reasonable temperature dependence of the hopping rate down to 300 K.

To estimate the “attempt frequencies” ν_a from our SIA migration data, we fit the hopping rates ν_h in Fig. 2 to the Arrhenius form⁵⁰

$$\nu_h = \nu_a e^{-\Delta E_m/k_B T} \quad (2)$$

at temperature $k_B T$ and with energy barrier ΔE_m . The fitted values for ν_a and ΔE_m are listed in Table II. Above room temperature, we find that all of our calculated ΔE_m are less than 0.1 eV. We also provide comparisons to previous direct calculations of migration energy barriers.^{4,18} We note that the hopping rates in Mo and V of 2–3 THz correspond to extremely short residence times of < 1 ps spent in each Wigner-Seitz cell.

The reliability of our calculated ΔE_m should be determined from our SIA formation energies, in Table I. In particular the differences between the $\langle 111 \rangle$ and other orientations are correctly ordered in all of our cases, except for V and Nb, which have an orientational degeneracy. For these two metals, the pseudopotential calculations find smaller ΔE_f differences than for Mo or Ta, but none of the previous works find a degenerate $\langle 111 \rangle$ energy, as we have for V. Also for Ta, the previous result¹⁸ for ΔE_m is higher than our value and this could be due to our underestimating the formation energies. Clearly our method does not have the same *ab initio* precision of the pseudopotential methods. We note, however, that the previous result for Ta,¹⁸ which seems

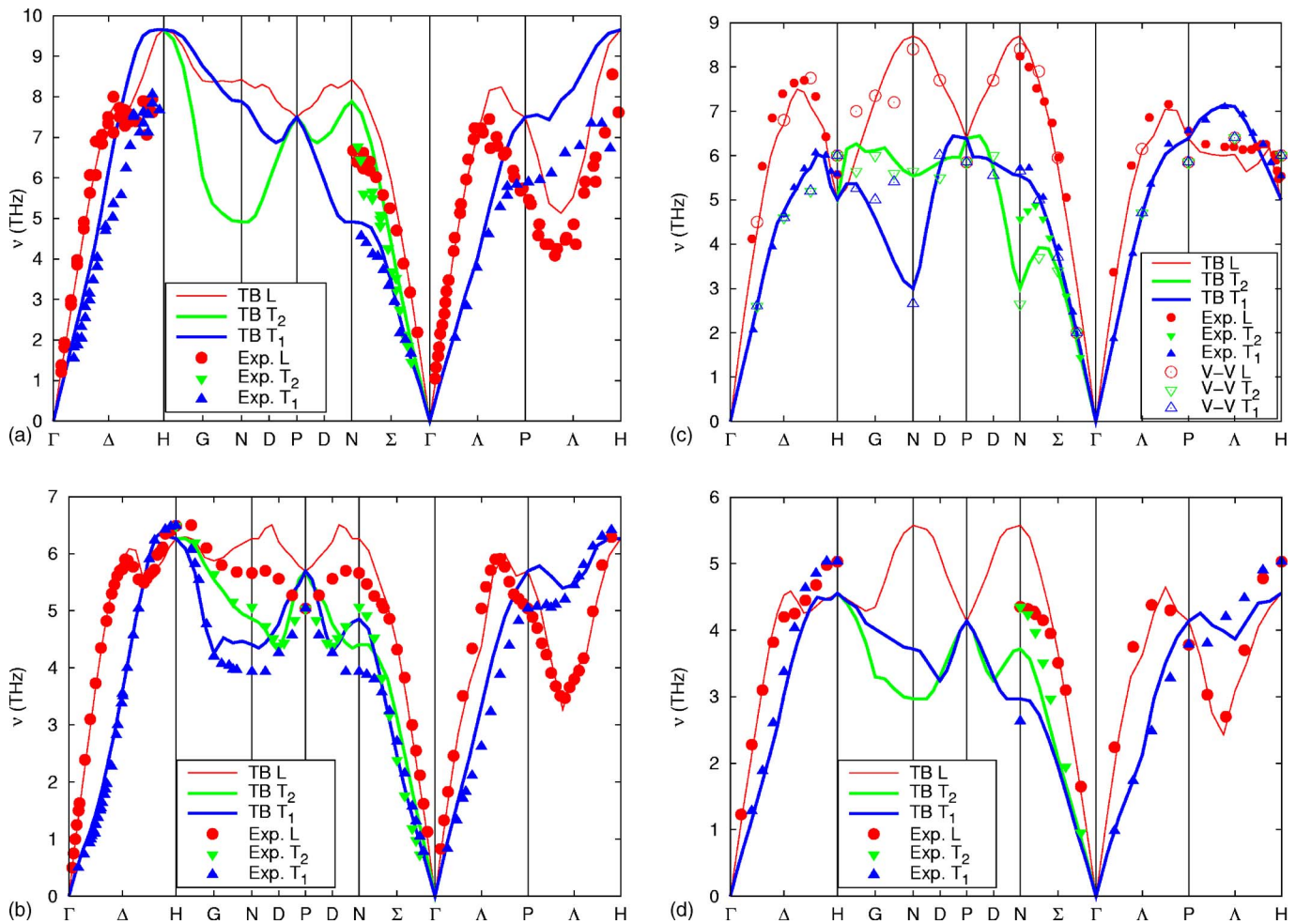


FIG. 5. (Color online) Calculated phonon dispersions compared to experiment (Exp., solid symbols) for (a) V,⁵⁵ (b) Nb,⁵⁶ (c) Mo,⁵⁷ and (d) Ta.⁵⁸ The calculations are based on the TB parametrization in Ref. 23. Thin (thick) solid lines give phonon dispersions for L (T) modes calculated by the frozen phonon method; for Mo, in addition, results obtained from molecular dynamics by the velocity autocorrelation method are shown (V-V, open symbols).

anomalously large compared to other bcc metals,⁴ used a supercell half the size of ours, which could result in an increased lattice strain. Finally, since much of our data for SIA's seem generic to the bcc transition metals, we point out that our results are most reliable for Mo, whose TB accuracy is similar to *ab initio* for all of the properties that we have checked.²³

At temperatures lower than those studied here, it is predicted that correlated hops dominate SIA motion—e.g., as shown for V via MD^{6,7}—and that correlated hops occur mostly along the high-symmetry directions. We find no similar theoretical treatment for Nb, but there do exist early experimental reports of uncommonly high and long-range migration rates of Nb SIA's at temperatures as low as 4.5 K.^{51–53} For this reason, we expect that our Arrhenius fits are valid for $T > 300$ K, but there may be a more complicated behavior due to correlated SIA hopping at very low temperatures.

While it is difficult to propose a single reason why SIA migration is so rapid, there are several observations that we can make based on our hopping data. We examined the atomic motions of SIA dumbbell pairs, both preceding and

during migration events, as shown for temperatures of 400 K in Fig. 3. In all cases, we find that the COM displacement and the bond length are at (or near) their maxima, just prior to most hopping events. Viewed in time, this motion appears as an “inchworm” process, whereby the dumbbell gradually pushes a leading atom towards the destination cell, via increasing extension of the bond length, while in response the lagging atom is pulled towards the cell center. This process pushes the COM further towards the destination cell. Notably, the COM has a low-frequency component that appears to be set primarily by the time between hops, as shown in Fig. 3(b) where the peaks and troughs of displacement are consistent with the hopping rate. In contrast, the rapid bond-length vibrations appear to be independent of the time between hops. Based on this, we initially hypothesized that the frequencies of the bond dilation gave an “attempt frequency” for SIA hopping. We will show, however, that the bond-length frequencies are approximately 30% too large to give the exact Arrhenius prefactors, even though the two frequencies are roughly proportional for all of the transition metals studied here.

B. Self-interstitial vibrations

It is apparent that the vibrational modes of the SIA dumbbell are important for SIA migration, as shown, e.g., by the time variation of the dumbbell bond length and COM in Fig. 3. We believe that the amplitudes of these vibrations respond to the migration events and vice versa. To analyze the trajectories calculated in our MD simulations, we show in Fig. 4 the calculated SIA vibrational spectra, along with the VDOS with and without SIA's. These spectra are obtained by Fourier transforms of an approximately 30-ps window of time-correlation functions, as described for the VAC method in Sec. II B. Additionally, the VDOS are scaled up by a factor of 128 in the tails to highlight the high-frequency SIA modes. We note that all of these tails should be perfectly flat for the perfect bcc metals, at high frequencies. However, using the VAC method, there is a small, decaying noise that is present even in the perfect bcc metal, arising from artifacts due to the finite time window of the Fourier transform and from anharmonicity. We note that this systematic, high-frequency noise can be reduced by increasing the time-sampling window or by filtering, but in the following we care mainly about the increase in spectra at high frequencies due to SIA's, so we analyze the raw data.

Comparing the dumbbell bond vibrations in each system, we see that the enhanced tail spectra due to SIA's are located at exactly the vibrational frequencies of the bond-stretching A_g mode. Notably, the high-frequency A_g modes of V and Nb are not as sharp, nor are they well defined, compared to Mo and Ta. The broadening of the tail peaks in V and Nb is likely due to the metastable $\langle 100 \rangle$ modes that were discussed in the preceding section, which can cause interference between competing modes. Nonetheless, for all of our bcc transition metals, the largest tail peaks from the A_g mode consistently occur at roughly twice the frequency of the VDOS peak for the perfect bcc system.

In contrast to the bond-stretching modes, the COM modes are lower in frequency and seem mostly spread out across the central VDOS spectra of the host lattice. Center-of-mass peaks lying just above and just below the host VDOS spectra are the primary features generic to all of our bcc metals. In particular, the high-frequency peaks just above the VDOS are similar to the Arrhenius prefactors that were fit in the preceding section (cross bars in Fig. 4). For comparison to the A_g modes at roughly $2\times$ the frequency of the bcc phonon density of states peak, the highest COM modes occur at $1.5\times$, and the corresponding Arrhenius prefactors also occur at roughly $1.5\times$, that same peak.

We find that in all cases the Arrhenius prefactors fall somewhat above the traditional cutoff frequencies of the host bcc lattices. Comparing to the SIA vibrational modes, these prefactors are approximately 70%–80% of the frequency of the SIA A_g modes, shown in Fig. 4 and listed in Table II. Since the presence of a SIA adds many new modes to the high-frequency portion of the VDOS spectra, it is reasonable that the Arrhenius prefactors are related to these new modes. Of course all of the prefactors that we have calculated should include other terms beyond the basic attempt frequency—e.g., the vibrational entropy term $\exp(\Delta S_{vib}/k_B)$ and other factors—but these calculations we leave for another communication.

One final, interesting application of our calculations is suggested by the experimental phonon spectra of HCP Fe.³¹ In HCP Fe at high pressure, the published experimental data show high-frequency noise and oscillations in the VDOS, at the same frequency range where we expect such behavior to occur due to a SIA or clusters of SIA's. However, unpublished experimental results following up on those measurements show less noise and no evidence of a high-frequency contribution.⁵⁴ To investigate the possibility of forming SIA's at high pressures, we calculated the excess volumes introduced by our SIA's. We found that a range of 0.1–0.5 excess atomic volumes were added by the SIA's, compared, by definition, to an equal number of bcc atoms. This suggests that any positive pressure should increase the free energy cost to introduce a SIA; hence, our calculations agree more with the recent, unpublished results finding no additional high-frequency component.⁵⁴ Based on this, we speculate that the best ways to observe the SIA VDOS in experiment would be under irradiation or under nonhydrostatic stress, which might favor SIAs oriented along selected directions. We note that all of our results are for individual SIA defects—i.e., ignoring clusters of SIA's—which are important for irradiated materials.¹⁴ Our single SIA results are helpful for describing the fast, one-dimensional glides that are important—e.g., in the initial stages of irradiation, when only single SIA's have formed.

IV. CONCLUSIONS

We have calculated self-interstitial dynamical properties from a tight-binding approximation of electronic structure. We have tested our method against experiment for phonon spectra and against previous *ab initio* results for self-interstitial formation energies. We find good agreement for the phonon spectra and for many self-interstitial formation energies, and in all nonmagnetic cases, we find a preferential alignment of self-interstitials along $\langle 111 \rangle$ directions; in contrast, we confirm the predicted $\langle 110 \rangle$ self-interstitial alignment in ferromagnetic Fe. By using a molecular-dynamics-based method for calculating velocity autocorrelations, we have identified the high-frequency vibrational modes for self-interstitials in bcc metals. These vibrations appear to be generic to the transition metals studied and occur up to twice the frequencies of the peaks of the perfect bcc phonon densities of states. For a quantitative comparison of self-interstitial mobilities for different systems, we have performed Arrhenius fits to high-temperature interstitial migration data. We find that interstitial hopping is mostly Arrhenius down to 300 K with energy barriers for diffusion on the order of 0.1 eV. Also the Arrhenius prefactors are centered at approximately $1.5\times$ the frequency of the phonon densities-of-states peak. Since the frequency prefactors lie above the bcc cutoff, we suggest that there is a contribution from the high-frequency interstitial vibrations to the migration kinetics. Our results also imply a potentially useful method for identifying self-interstitials—namely, from spectroscopic measurement of localized interstitial vibrational modes, a phenomenon that is perhaps important in Fe under applied stress³¹ and in other bcc transition metals.

ACKNOWLEDGMENTS

We acknowledge the support of the U.S. Naval Research Laboratory, the Office of Naval Research, and the DOD HPCMPO CHSSI program. We also acknowledge a fruitful discussion with S. J. Putterman on defects in metals at high pressure.

APPENDIX: TEST OF TIGHT-BINDING
PARAMETRIZATION

Previous TB parametrization for V, Nb, Mo, and Ta is discussed in Ref. 23. For the cases of Ta and Mo, our original parametrization was stable for all SIA structures and gave a favorable comparison to experiment for the phonon dispersion, as shown in Figs. 5(c) and 5(d).^{55–58} These results were calculated here by the frozen-phonon method, as discussed, e.g., in Refs. 22 and 23, and by the velocity-autocorrelation method, as discussed in the text and in Ref. 49. The velocity-autocorrelation method overestimates some phonon frequencies—e.g., at the H point for Mo in Fig. 5(c), which is a result of long-range interactions and finite-size effects, as noted previously.⁵⁹ For the cases of V and Nb,⁶⁰ our original parametrization was unstable to close separation and required the inclusion in the fit of additional reduced-lattice-constant structures to fully describe the SIA interaction. Results based on current parameters for V and Nb are shown in Figs. 5(a) and 5(b).

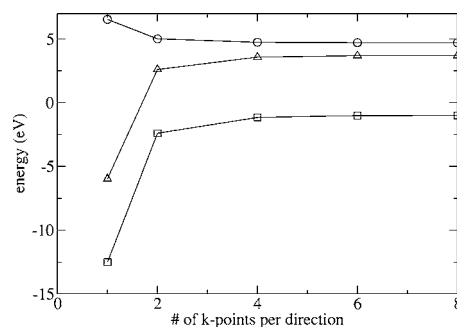


FIG. 6. k -point convergence for a Nb bcc 128-atom repeated cell (square) with self-interstitial (triangle) and the difference [self-interstitial formation energy from Eq. (1), circles].

The new parameter fits²⁸ were performed using a database of LAPW calculations, with Hedin-Lundqvist⁶¹ parametrization of the LDA.³⁸ In addition, energies at close separation were included, down to 60% of the equilibrium neighbor spacing, as occurs naturally for the SIA during MD runs. Structures included in the fits were bcc, fcc, and simple cubic. For static SIA formation energies, a Monkhorst-Pack k mesh⁴³ with four k points per direction was used for all systems, based on our convergence studies for Nb (Fig. 6). No experimental data were used to determine the parameters of our TB model.

*Electronic address: daniel.kris@gmail.com

- ¹P. G. Lucasson and R. M. Walker, Phys. Rev. **127**, 485 (1962).
- ²J. F. W. Young, J. Nucl. Mater. **69/70**, 310 (1978).
- ³K. Nordlund and R. S. Averback, Phys. Rev. Lett. **80**, 4201 (1998).
- ⁴S. Han, L. A. Zepeda-Ruiz, G. J. Ackland, R. Car, and D. J. Srolovitz, Phys. Rev. B **66**, 220101(R) (2002).
- ⁵L. A. Zepeda-Ruiz, S. Han, D. J. Srolovitz, R. Car, and B. D. Wirth, Phys. Rev. B **67**, 134114 (2003).
- ⁶L. A. Zepeda-Ruiz, J. Rottler, S. Han, G. J. Ackland, R. Car, and D. J. Srolovitz, Phys. Rev. B **70**, 060102(R) (2004).
- ⁷L. A. Zepeda-Ruiz, J. Rottler, B. D. Wirth, R. Car, and D. J. Srolovitz, Acta Mater. **53**, 1985 (2005).
- ⁸D. Nguyen-Manh, A. P. Horsfield, and S. L. Dudarev, Phys. Rev. B **73**, 020101(R) (2006).
- ⁹B. D. Wirth, G. R. Odette, D. Maroudas, and G. E. Lucas, J. Nucl. Mater. **244**, 185 (1997).
- ¹⁰N. Soneda and T. D. Rubia, Philos. Mag. A **81**, 331 (2001).
- ¹¹C. Domain and C. S. Becquart, Phys. Rev. B **65**, 024103 (2001).
- ¹²J. Marian, B. D. Wirth, A. Caro, B. Sadigh, G. R. Odette, J. M. Perlado, and T. Diaz dela Rubia, Phys. Rev. B **65**, 144102 (2002).
- ¹³C.-C. Fu, F. Willaime, and P. Ordejon, Phys. Rev. Lett. **92**, 175503 (2004).
- ¹⁴C.-C. Fu, J. Torre, F. Willaime, J.-L. Bocquet, and A. Barbu, Nat. Mater. **4**, 68 (2005).
- ¹⁵P. N. Ram, Phys. Rev. B **43**, 6977 (1991).
- ¹⁶J. A. Blah, S. S. Pohlong, and P. N. Ram, Phys. Rev. B **49**, 15055

(1994).

- ¹⁷W. Xu and J. A. Moriarty, Phys. Rev. B **54**, 6941 (1996).
- ¹⁸L. H. Yang, P. Soderlind, and J. A. Moriarty, Philos. Mag. A **81**, 1355 (2001).
- ¹⁹M. H. Carlberg, E. P. Munger, and L. Hultman, J. Phys.: Condens. Matter **11**, 6509 (1999).
- ²⁰M. H. Carlberg, E. P. Munger, and L. Hultman, J. Phys.: Condens. Matter **12**, 79 (2000).
- ²¹K. Kusunoki, in *Proceedings of the Fourth International Conference on Supercomputing in Nuclear Applications* (SNA, Tokyo, 2000) (CD ROM proceedings).
- ²²R. E. Cohen, M. J. Mehl, and D. A. Papaconstantopoulos, Phys. Rev. B **50**, 14694 (1994).
- ²³M. J. Mehl and D. A. Papaconstantopoulos, Phys. Rev. B **54**, 4519 (1996).
- ²⁴M. J. Mehl and D. A. Papaconstantopoulos, in *Topics in Computational Materials Science*, 1st ed., edited by C. Fong (World Scientific, Singapore, 1998), Vol. 1, Chap. 5, pp. 169–213.
- ²⁵D. A. Papaconstantopoulos and M. J. Mehl, J. Phys.: Condens. Matter **15**, R413 (2003).
- ²⁶M. J. Mehl and D. A. Papaconstantopoulos, in *Handbook of Materials Modeling*, 1st ed., edited by S. Yip (Springer, Amsterdam, 2005), Vol. 1, p. 275.
- ²⁷D. A. Papaconstantopoulos and M. J. Mehl, in *Encyclopedia of Condensed Matter Physics*, edited by G. Bassani (Elsevier, Oxford, 2005), Vol. 6, p. 194.
- ²⁸The parameters used in this paper are available from the authors or at <http://cst-www.nrl.navy.mil/bind/>.

- ²⁹F. Kirchhoff, M. J. Mehl, N. I. Papanicolaou, D. A. Papaconstantopoulos, and F. S. Khan, *Phys. Rev. B* **63**, 195101 (2001).
- ³⁰More details about the DOD-parallel tight-binding molecular-dynamics code can be found at URL: <http://cst-www.nrl.navy.mil/bind/dodtb/>.
- ³¹H. K. Mao *et al.* *Science* **292**, 914 (2001).
- ³²R. Bullough and R. C. Perrin, *Proc. R. Soc. London, Ser. A* **305**, 541 (1968).
- ³³H. R. Paneth, *Phys. Rev.* **80**, 708 (1950).
- ³⁴M. S. Daw and M. I. Baskes, *Phys. Rev. Lett.* **50**, 1285 (1983).
- ³⁵M. S. Daw and M. I. Baskes, *Phys. Rev. B* **29**, 6443 (1984).
- ³⁶L. Malerba, D. Terentyev, P. Olsson, R. Chakarova, and J. Wallenius, *J. Nucl. Mater.* **329-333**, 1156 (2004).
- ³⁷M. W. Finnis and J. E. Sinclair, *Philos. Mag. A* **50**, 45 (1984).
- ³⁸W. Kohn and L. Sham, *Phys. Rev.* **140**, A1133 (1965).
- ³⁹O. K. Andersen, *Phys. Rev. B* **12**, 3060 (1975).
- ⁴⁰D. Singh, H. Krakauer, and C. S. Wang, *Phys. Rev. B* **34**, 8391 (1986).
- ⁴¹M. L. Cohen and T. K. Bergstresser, *Phys. Rev.* **141**, 789 (1966).
- ⁴²C. M. Goringe, D. R. Bowler, and E. Hernandez, *Rep. Prog. Phys.* **60**, 1447 (1997).
- ⁴³H. J. Monkhorst and J. D. Pack, *Phys. Rev. B* **13**, 5188 (1976).
- ⁴⁴N. W. Ashcroft and N. D. Mermin, *Solid State Physics*, 1st ed. (Saunders College Publishing, Fort Worth, 1976).
- ⁴⁵D. Finkenstadt and D. D. Johnson, *Phys. Rev. B* **73**, 024101 (2006).
- ⁴⁶C. E. Lekka (private communication).
- ⁴⁷*CRC Handbook of Chemistry and Physics, Internet Version 2006*, 86th ed., edited by D. R. Lile (Taylor & Francis, Boca Raton, FL, 2006), Chap. 12, pp. 12–196 in table, “Thermal and Physical Properties of Pure Metals.”
- ⁴⁸J. M. Dickey and A. Paskin, *Phys. Rev.* **188**, 1407 (1969).
- ⁴⁹C. Z. Wang, A. Fasolino, and E. Tosatti, *Phys. Rev. B* **37**, 2116 (1988).
- ⁵⁰D. A. Porter and K. E. Easterling, *Phase Transformations in Metals and Alloys*, 2nd ed. (Stanley Thornes Ltd, London, 1992).
- ⁵¹F. Dausinger, J. Fuss, J. Schweikhardt, and H. Schultz, *J. Nucl. Mater.* **69–70**, 689 (1978).
- ⁵²J. Fuss and H. Schultz, *Radiat. Eff.* **40**, 181 (1979).
- ⁵³P. Hautojarvi, H. Huomo, P. Saariaho, A. Vehanen, and J. Yli-Kauppila, *J. Phys. F: Met. Phys.* **13**, 1415 (1983).
- ⁵⁴V. V. Struzhkin (private communication).
- ⁵⁵R. Colella and B. W. Batterman, *Phys. Rev. B* **1**, 3913 (1970).
- ⁵⁶Y. Nakagawa and A. D. B. Woods, *Phys. Rev. Lett.* **11**, 271 (1963).
- ⁵⁷A. D. B. Woods and S. H. Chen, *Solid State Commun.* **2**, 233 (1964).
- ⁵⁸A. D. B. Woods, *Phys. Rev.* **136**, A781 (1964).
- ⁵⁹H. Haas, C. Z. Wang, K. M. Ho, M. Fahnle, and C. Elsasser, *J. Phys.: Condens. Matter* **11**, 5455 (1999).
- ⁶⁰C. E. Lekka, M. J. Mehl, N. Bernstein, and D. A. Papaconstantopoulos, *Phys. Rev. B* **68**, 035422 (2003).
- ⁶¹L. Hedin and B. I. Lundqvist, *J. Phys. C* **4**, 2064 (1971).